Pickering emulsions stabilized by inside/out Janus nanotubes: Oil triggers an evolving solid interfacial layer

Estelle Puel, Céline Cau Dit Coumes, Arnaud Poulesquen, Fabienne Testard, Antoine Thill

Journal of Colloid and Interface Science 647 (2023) 478–487

Contents lists available at ScienceDirect

Journal of Colloid And Interface Science

journal homepage: www.elsevier.com/locate/jcis

Pickering emulsions stabilized by inside/out Janus nanotubes: Oil triggers an evolving solid interfacial layer

Estelle Puel [a], Céline Cau Dit Coumes [b], Arnaud Poulesquen [b], Fabienne Testard [a], Antoine Thill [a,*]

[a] Université Paris-Saclay, CEA Saclay, CNRS, NIMBE, UMR 3685, LIONS, 91191 Gif-Sur-Yvette Cedex, France
[b] CEA, DES, ISEC, DE2D, Université Montpellier, Marcoule, 30207 Bagnols-Sur-Cèze Cedex, France

GRAPHICAL ABSTRACT

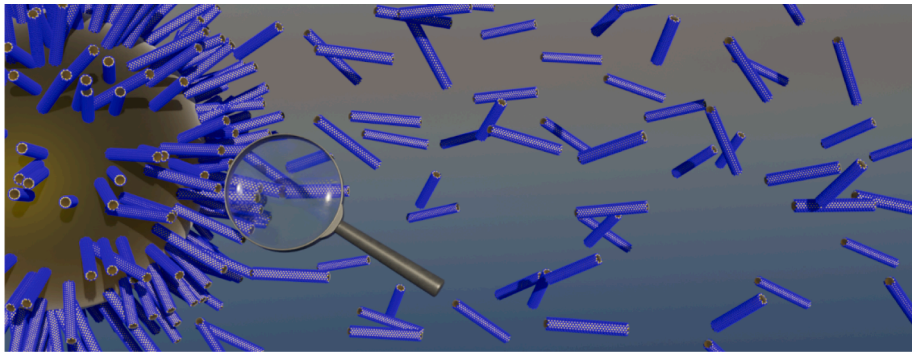

ARTICLE INFO

Keywords:
Pickering emulsions
Hybrid imogolites
Interfacial properties
Janus nanotubes
Gel oil network

ABSTRACT

Hypothesis: In the field of Pickering emulsion, original inside/ouside Janus clays nanoparticles are investigated for their emulsification properties. Imogolite is a tubular nanomineral of the clay family having both inner and outer hydrophilic surfaces. A Janus version of this nanomineral with an inner surface fully covered by methyl groups can be obtained directly by synthesis (Imo-CH_3, hybrid imogolite). The hydrophilic/hydrophobic duality of the Janus Imo-CH_3 allows the nanotubes to be dispersed in an aqueous suspension and enables emulsification of non-polar compounds due to the hydrophobic inner cavity of the nanotube.
Experiments: Through the combination of Small Angle X-ray Scattering (SAXS), interfacial observations and rheology, the stabilization mechanism of imo-CH_3 in oil-water emulsions has been investigated.
Findings: Here, we show that interfacial stabilization of an oil-in-water emulsion is rapidly obtained at a critical Imo-CH_3 concentration as low as 0.6 wt%. Below this concentration threshold, no arrested coalescence is observed, and excess oil is expelled from the emulsion through a cascading coalescence mechanism. The stability of the emulsion above the concentration threshold is reinforced by an evolving interfacial solid layer resulting

Abbreviations: Imo-CH_3, hybrid imogolite; $r_{imo\text{-}ext}$, external radius of Imo-CH_3; $r_{imo\text{-}int}$, internal radius of Imo-CH_3; l_{imo}, average length of Imo-CH_3; NR, nile Red; Φ_e, emulsion volume fraction; Φ_o, initial oil volume fraction $\Phi_o = V_{oil}/(V_{oil} + V_{water})$; Φ_o^e, oil volume fraction in the emulsion phase $\Phi_o^e = V_{oil}/V_{emulsion}$ or $\Phi_o^e = \Phi_o/\Phi_e$; Φ_j, experimental maximum packing of the emulsion $\Phi_j = 0.64$.

* Corresponding author.
E-mail address: antoine.thill@cea.fr (A. Thill).

https://doi.org/10.1016/j.jcis.2023.04.102
Received 5 December 2022; Received in revised form 19 April 2023; Accepted 21 April 2023
Available online 15 May 2023

from the aggregation of Imo-CH_3 nanotubes that is triggered by the penetration of confined oil front into the continuous phase.

1. Introduction

The dispersion of oil in water is normally hindered by the high interfacial energy between the two phases. Emulsification can be obtained, however, using different strategies such as reducing the interfacial tension, creating an energy barrier to coalescence, and the global rheological properties of the continuous phase, by modifying, for example, the emulsifier concentration [1–5]. Among the different approaches for emulsification, so-called Pickering emulsions are obtained using solid particles that adsorb at the oil/water interface [6,7]. The adsorption energy of partially wetted solid nanoparticles is controlled by the interfacial energy and can be very high compared to thermal energy, making them almost irreversibly attached to the interface [8,9]. This leads to long lasting metastability and interesting properties like arrested coalescence, where the average size of the emulsified droplets is essentially controlled by the initial concentration of solid nanoparticles [10,11]. A wide range of possible nanomaterials (solid, soft-matter based, hybrid, Janus) has been explored and the mechanisms explaining the stability have been reviewed [3,5,12–31].

In the present article, we focus on emulsions stabilized by a special type of hybrid nanotubes, which form an inside/out Janus system (hybrid imogolite) [32,33]. Imogolite is a natural clay nanomineral formed through the weathering of volcanic rocks [34]. A few years after its discovery in Japanese volcanic soils, it was demonstrated that a synthetic material very similar to the natural clay nanotubes could be obtained through co-precipitation of aluminum and silicon [35–38]. Recently, in 2011, the research group of Barbara Bonelli proposed a modified synthesis where the silicon precursor (generally tetraethoxysilane) is replaced by methyltriethoxysilane leading in one step to hybrid nanotubes (referred hereafter as Imo-CH_3) having a similar external surface to as the natural nanoclay but with a strongly hydrophobic nanocavity [39]. The hybrid nanotubes have an outer diameter of 3 nm and an internal hydrophobic cavity of ~ 2 nm representing an internal nanoporous volume of 0.1 $cm^3 \cdot g^{-1}$. Contrary to many systems, Imo-CH_3 are intrinsically Janus and do not require the use of additional surfactants or adsorbed molecules to acquire their surface activity.

Interestingly, it has been observed by Small Angle X-ray Scattering (SAXS) that under ambient pressure and temperature conditions, these hybrid nanotubes are not filled by liquid water. The internal electron density determined by SAXS is between 50 and 100 $e^- \cdot nm^{-3}$, while liquid water is 330 $e^- \cdot nm^{-3}$. In turn, it has been observed that the internal cavity can be filled by poorly water-soluble molecules [40]. Since then, a wide range of molecules have been successfully introduced inside the Imo-CH_3 hydrophobic cavity, such as alcohols, solvents and dyes [41–43], when put in contact with oil, the Imo-CH_3 nanotubes become filled with oil [44].

These favorable interactions with hydrophobic molecules and phases motivated experiments for their use in the stabilization of emulsions. The ability of these Janus nanotubes to stabilize Pickering emulsion was first demonstrated by Picot *et al.* [44]. However, the stabilization mechanism was not clearly established. Here, we further explore the stabilization mechanism using model oil phases (the alkanes: hexadecane or dodecane) in contact with Imo-CH_3 dispersions. The selection of alkanes is justified by their chemical nature. They are made up of long aliphatic chains without any reactive chemical functional groups that could influence the results. In this paper, hybrid imogolites nanotubes (Imo-CH_3) were synthesized, characterized and used to stabilize Pickering emulsions. The adsorption and evolution of the interfacial tension between alkane and Imo-CH_3 suspensions were investigated as a function of time. Our results demonstrate that metastable, yet fragile emulsions are rapidly formed and continue to evolve through oil-triggered reinforcement of their stability. Finally, we demonstrate through energetic approach the stabilization mechanism of emulsification obtained with original inside/ouside Janus clays nanoparticles.

2. Materials and methods

Aluminium-tri-*sec*-butoxide (97 % purity), Hydrochloric acid 37 %, Trimethoxymethylsilane (95 % purity), Hexadecane (Reagent plus®, 99 %) and Dodecane (≥99.0 %) were purchased from Sigma Aldrich and used as received. Milli-Q water at 18 MΩ·cm was used for synthesis and emulsification tests.

2.1. Synthesis of hybrid imogolites nanotubes

Hybrid imogolites, shown in **Figure S1**, are synthesized using a protocol inspired by Picot *et al.* and Bottero *et al.* [39,45]. Aluminum-tri-*sec*-butoxide is dissolved in a hydrochloric acid solution with a HCl/Al molar ratio of 0.5. Trimethoxymethylsilane is then added to this solution under vigorous steering until a Si/Al molar ratio of 0.6 is reached. The solution is kept under stirring for 1 h at room temperature, and then it is placed in an oven at 90 °C for 5 days. After cooling, the solution is dialyzed using 6–8 k_D membranes until the dialysis water reaches a conductivity of 10 $\mu S.cm^{-1}$. The final aqueous suspension of Imo-CH_3 appears slightly turbid and is birefringent. The mass concentration of the dialyzed suspension is 6000 $g.m^{-3}$, or 0.6 wt%, as determined by weighing the sample after drying in an oven at 50 °C. The suspension is used directly as synthesized, diluted with MilliQ water, or dried and redispersed when required. To obtain a concentration higher than 0.6 wt %, the suspension is spray-dried with a Buchi b290 mini spray dryer in order to obtain a powder that can be redispersed in water. The drying parameters are: temperature 170 °C, aspiration 100 %, pump 30 % and gas flow at 473 $l.h^{-1}$. It was verified that the dried powder leads to the same suspension properties as those obtained from the dialyzed suspension. The imogolite suspensions were characterized by InfraRed (IR) spectroscopy, SAXS and viscosimetry (**Figure S2**, **Figure S3** **and Table S1)**. In particular, we have obtained the characteristic dimensions of Imo-CH_3, such as the external radius, $r_{imo-ext}$, equal to 1.54 nm, the internal radius, $r_{imo-int}$, equal to 0.93 nm and the average length, l_{imo}, equal to 290 nm. For further information, see **Tables S1 to S3**.

2.2. Preparation of Pickering emulsions stabilized using hybrid imogolites

Emulsions were prepared by mixing aqueous suspensions of Imo-CH_3 and hexadecane in 5 mL glass containers with an Ultra-Turrax model T10 overhead stirrer (IKA). The impact of mixing time and mixing power was initially studied using a oil/water mixture of 40 % by volume of oil and 0.6 wt% (initial concentration obtained after the synthesis) Imo-CH_3 in the water phase. Then, the oil/water volumetric fraction was varied between 0 and 80 % by volume, and the concentration of Imo-CH_3 in the water phase was varied between 0 and 2 wt% with a fixed mixing condition of 3 min at 25,000 rpm for a total volume of 5 mL. For imogolite concentrations above 0.6 wt%, the aqueous imogolite suspensions were prepared from redispersed spray-dried powders.

2.3. Small angle X-ray scattering

Small- and wide-angle X-ray scattering (SAXS/WAXS) data were acquired on a XEUSS 2.0 instrument (XENOCS) at the University Paris-Saclay SWAXS Laboratory. X-rays were produced from a Cu microfocus X-ray source and collimated with scatter-less slit technology. Scattered X-rays were collected on a Pilatus 1 M detector (Dectris). SAXS and

WAXS analysis were performed, respectively, under high resolution or high flux mode. The sample-to-detector distances (19.2 cm for wide angles and 250 cm for small angles), calibrated with silver behenate, provided a large q-range of 3.8 × 10^{-3} to 2.7 $Å^{-1}$. The detector count was normalized into the differential cross section from a direct beam measurement after a classical radial averaging procedure using the in-house open-source pySAXS software [46,47]. The scattered intensity I (q) was plotted as a function of the amplitude of the scattering vector $q = \frac{4\pi \sin(\theta)}{\lambda}$, where 2θ is the scattering angle and λ is the wavelength.

The samples were analyzed in 1.5 mm borosilicate capillaries (Hilgenberg). Scattering intensities were recorded at room temperature and under secondary vacuum to minimize interactions between the X-ray beam and air. The typical acquisition time was 1800 s.

2.4. Confocal laser scanning microscope

Fluorescence images were obtained with an Olympus IX81 confocal laser scanning microscope equipped with a Fluoview-1000 confocal head operating at ×40 magnification. Observations were performed with excitation wavelengths of 488 nm (Ar) and 543 nm (HeNe(G)). For the confocal experiments, the emulsions were prepared with a solvatochromic dye, Nile Red (NR), dispersed in the oil phase. Nile Red has an environmentally-dependent excitation wavelength. In hexadecane, NR has an excitation maximum at 488 nm and a fluorescence emission maximum at 530 nm (reported in **Figure S4**). When NR is encapsulated inside Imo-CH_3 nanotubes, its excitation maximum is red-shifted to 543 nm and its fluorescence emission is at 620 nm. This important solvatochromic shift makes it possible to characterize the water and oil domains inside the emulsion with a single dye. Confocal microscopy was performed at room temperature by placing a drop of the emulsion in a 1.3 mm depth demontable UV quartz cuvette from Hellma.

2.5. Interfacial tension measurements

Drop observations and interfacial tension measurements were made using a Drop Shape Analyzer (DSA 25, KRUSS GmbH, Germany). These data were processed using the Advance Surface software, equipped with a Young-Laplace analysis model. Experiments were performed at room temperature using pendant drop techniques. Drop formation was controlled by software, where a 1.5 mm diameter steel needle was used to form 30 μL drops of hybrid imogolite suspensions directly into a surrounding alkane (dodecane) phase. Beforehand, the dodecane was filled into an optical glass cell. For these experiments, dodecane was preferred to avoid the crystallization of hexadecane at a temperature lower than 18 °C.

2.6. Rheology

Rheological measurements were performed using a stress-controlled Anton Paar MCR 302 rheometer using a plate/plate geometry (diameter of 40 mm). The emulsions (40 $\%_{v/v}$ of 2.5 wt% Imo-CH_3 in water and 60 $\%_{v/v}$ of hexadecane) were prepared by vigorously stirring (25,000 rpm) with an Ultra-Turrax (IKA) and then delicately transferred to the rheometer using a pipette. Three emulsions were each studied using three different rheometer programs. Among these emulsions, one was used directly after preparation, whereas the two others were aged at room temperature. The first program was a time sweep, which helps to relax the strain, that was executed for 60 s with a strain of 5.0 × 10^{-4} and an angular frequency of 10 rad·s^{-1} (reported in **Figure S5a**). To confirm the solid elastic behavior of the material, a frequency sweep was executed with a strain of 5.0 × 10^{-4} and an angular frequency range from 100 to 0.1 rad·s^{-1} (reported in **Figure S5b**), followed by a final strain sweep at 1 rad·s^{-1} from 1.0 × 10^{-4} to 1 (0.01 to 100 %).

3. Results and discussion

3.1. Stability and aging of emulsions stabilized by Imo-CH_3 nanotubes

First, 60 $\%_{v/v}$ of an aqueous suspension of Imo-CH_3 (at 0.6 wt%) was mixed with 40 $\%_{v/v}$ of hexadecane to test the energy required for total oil emulsification **(Figure S6)**. These initial tests for the proper mixing conditions reveal a minimum stirring speed of 20,000 rpm (Ultra-Turrax) required to stabilize the emulsions. Below this speed, poor emulsification is observed, where the oil and water phases are not sufficiently dispersed to produce small enough droplets onto which the Imo-CH_3 nanotubes can adsorb. However, once the appropriate mixing energy is reached and when Imo-CH_3 is present in excess, complete emulsification is obtained regardless of the mixing time, even after only 30 s. Thus, for these conditions, the mixing time is not a key parameter **(Figure S7)**. We, therefore, selected a mixing condition of 3 min at 25,000 rpm to explore all the emulsification formulations.

The emulsions were characterized by confocal laser scanning microscopy after 24 h of rest (see Materials and methods: *Confocal laser scanning microscope*) using a solvatochromic dye. The results presented **in** Fig. 1 show the formation of a direct emulsion (O/W). The drops with the characteristic fluorescence emission of Nile Red (NR) in non-polar solvent contain the oil (Fig. 1**c**). They are surrounded by an aqueous suspension characterized by the typical fluorescent signature of NR encapsulated in Imo-CH_3, (Fig. 1**b**). It is important to note that the red color is not limited to the oil/water interface but it spreads all over the continuous phase. This point will be discussed in detail later. The drops had a spherical morphology and were in the range of 5 to 70 μm in diameter with an average diameter of 25 μm determined by image analysis of over more than 1000 drops.

We next explored the maximum oil volume fraction with which it is possible to form a stable emulsion using a 0.6 wt% Imo-CH_3 suspension. Fig. 2 shows a picture of 5 mL vials taken after 24 h under rest, demonstrating that emulsification was obtained with up to 60 $\%_{v/v}$ of oil. The less dense emulsified droplets creamed toward the top of the vial and form a metastable emulsion volume quickly after stirring (approximately ten minutes). No visible evolution of this emulsion volume was observed even after months at rest. A slight turbidity of the water phase due to Imo-CH_3 was observed in the vials. This turbidity decreases as the volume fraction of oil increases. This results from the increasing transfer of the imogolite from the water phase to the emulsion phase. We can thus conclude that at low oil volume fraction, the Imo-CH_3 nanotubes are in excess with respect to the quantity required for stabilizing the emulsion. From Fig. 2**a**, the relative heights of the emulsion phase and total phases allow the calculation of Φ_e, the emulsion volume fraction, as a function of Φ_o the initial oil volume fraction (Fig. 2**b**). It is also possible to calculate Φ_o^e the oil volume fraction in the emulsion phase (equal to $V_{oil}/V_{emulsion}$ or Φ_o/Φ_e). After creaming, Φ_o/Φ_e reaches an experimental maximum packing of the emulsion denoted Φ_j. From Fig. 2**b**, the relationship between Φ_e and Φ_o is a straight line described by the equation $\Phi_e = \frac{1}{\Phi_j} = \Phi_o = 1.56\Phi_o$. The value of $\Phi_j = 0.64$ is found, which is close to the theoretical expected maximum random jamming limit of hard sphere packing [48–51]. The jamming limit for a polydisperse emulsion has been measured by confocal microscopy by Clusel et al. [52]. They found a value of 0.66. The droplets are thus efficiently stabilized and cream until they are as closely packed as possible. Emulsification is impossible for oil volume fractions above Φ_j ($\Phi_{oilmax} = \Phi_j$), as indicated by the dashed line in Fig. 2**b**. Indeed, for 70 and 80 $\%_{v/v}$, there was not enough continuous phase to accommodate randomly packed oil droplets and the system was destabilized with an excess oil concentration at 70 % by volume and prevented from forming an emulsion entirely at 80 $\%_{v/v}$. We can conclude that, in all conditions, the emulsions were at their packing limit and the oil droplets behaved as hard spheres.

Next, the impact of the hybrid imogolite concentration and the initial oil volume fraction on emulsion formulation was explored. The

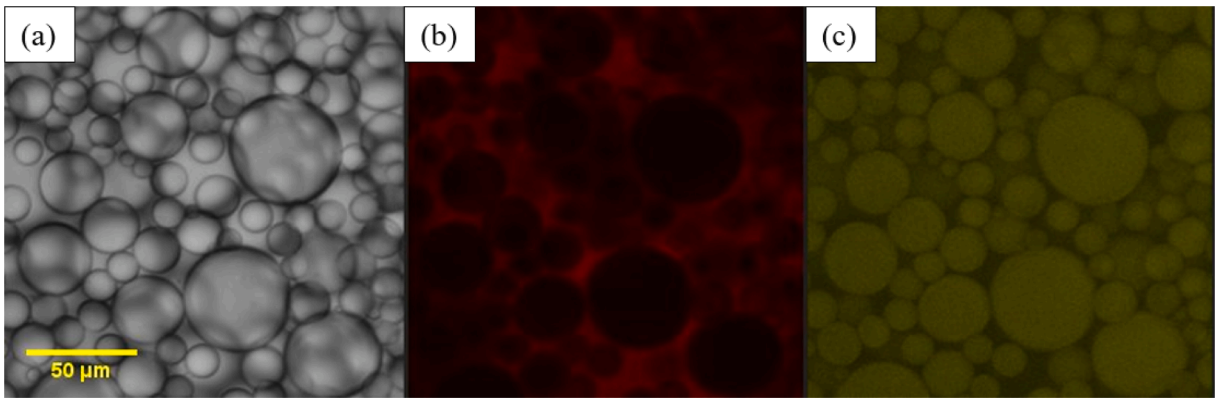

Fig. 1. Observation of an emulsion made from mixing (3 min at 25,000 rpm) 60 $\%_{v/v}$ of 0.6 wt% Imo-CH_3 water suspension and 40 $\%_{v/v}$ of hexadecane. (a) Transmitted light direct observation and Confocal micrographs of emulsions: (b) suspension of Imo-CH_3 domains (with excitation at 543 nm and emission at 620 nm), and (c) oil domains (with excitation at 488 nm and emission at 530 nm).

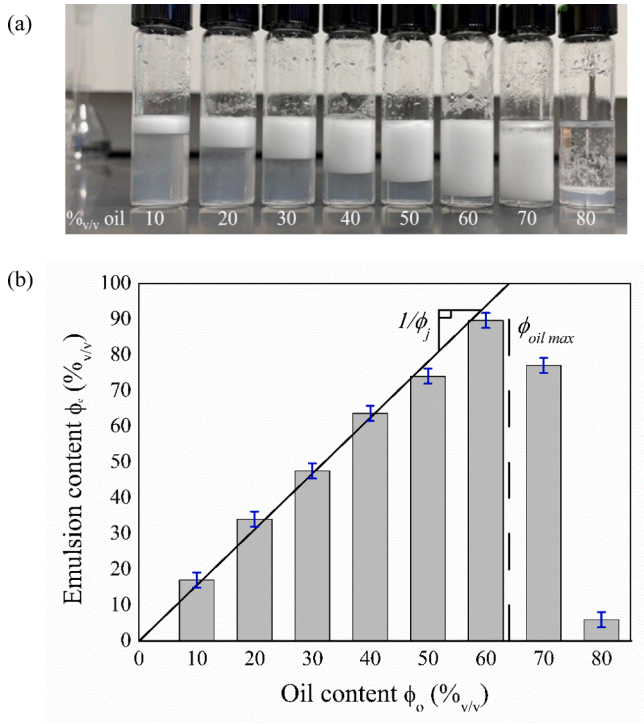

Fig. 2. Emulsions containing an aqueous suspension of hybrid imogolites and hexadecane. (a) Photograph of vials containing emulsions with oil fractions from 10 to 80 % by volume. (b) Graph of the emulsion content ($\%_{v/v}$) as a function of the initial oil content ($\%_{v/v}$) for a constant total volume. The dashed line corresponds to the maximum packing after creaming of the emulsion. The slope of the straight line represents the inverse of the maximum packing of the emulsion ($\Phi_j = 0.64$), which is close to the theoretical maximum random jamming limit [48–51].

metastability domains of incorporated oil in the emulsion (total or partial) are summarized in Fig. 3.

As discussed previously, full emulsification of the oil is not possible with spherical droplets for an oil volume fraction above the Φ_j limit of 0.64. Above this value, there is not enough available continuous phase for emulsification. The only possibility to go beyond this limit is to consider droplet deformations like those observed in some Pickering HIPE emulsions [53]. However, this was not observed by confocal microscopy for the studied system, where all droplets in all emulsions retained a spherical shape (Fig. 1). For emulsions prepared with initial oil volume fractions of 30, 40 or 50 $\%_{v/v}$, an imogolite concentration

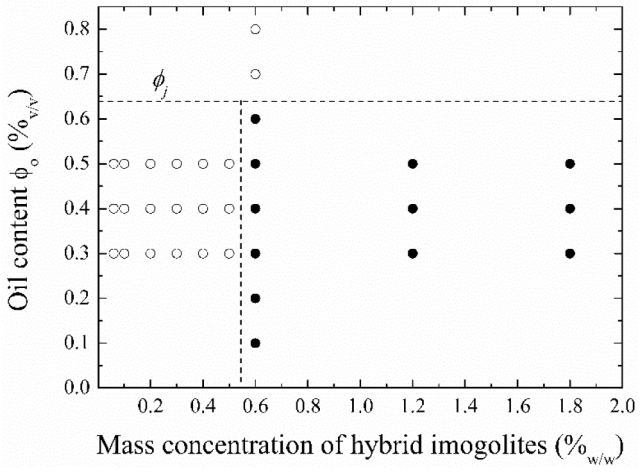

Fig. 3. Stability diagram of the emulsions stabilized by Imo-CH_3. Black circles correspond to samples with no excess oil and white circles to samples with no emulsification or with an observed excess oil layer. The horizontal dotted line corresponds to $\Phi_j = 0.64$, the maximum packing limit of oil drops in the emulsion.

threshold of between 0.5 and 0.6 wt% was observed (Fig. 3). Below this threshold, an excess oil layer was always observed after 24 h at rest, and above this threshold fully creamed emulsions were always observed.

The threshold concentration of Imo-CH_3 corresponds to the coverage of the oil droplet surface, at which the coalescence process is blocked. If the concentration is reduced, the stabilization provided by the nanotubes is not sufficient to prevent droplet coalescence and emulsification fails. This minimum Imo-CH_3 concentration depends on the total oil–water interfacial area, which is equal to $3V_o/R_d$, with V_o the average volume of an oil droplet and R_d the average radius of the emulsified droplets. For anisotropic objects like Imo-CH_3, the minimum mass concentration of Imo-CH_3 nanotubes to fully cover the oil–water interface strongly depends on their orientation at the interface. Indeed, we can estimate the mass coverage per surface unit (τ_w) for hybrid imogolites in the perpendicular or parallel orientation (**Figure S8**).

For a perpendicular orientation, this number scales as given by Eq (1):

$$\tau_{w-perpendicular} = \frac{m_{imo}^{unit} l_{imo}}{\pi\, r_{imo-ext}^2} \quad 0.47\ g{\cdot}m^{-2} \tag{1}$$

where m_{imo}^{unit} ($=1.2 \times 10^{-11} g.m^{-1}$) is the mass per unit length of the Imo-CH_3 nanotubes, l_{imo}($=290$ nm) is their average length and $r_{imo-ext}$

(=1.54 nm) is the external radius of the nanotube (see Materials and methods: *Synthesis of hybrid imogolites nanotubes* and **Tables S1 to S3**).

For a parallel orientation, this number scales as given by Eq(2):

$$\tau_{w-parallel} = \frac{m_{imo}^{unit}}{2\, r_{imo-ext}\, l_{imo}} \quad 3.9 \times 10^{-3}\ g{\cdot}m^{-2} \qquad (2)$$

The minimum concentration ratio between a perpendicular and parallel organization given by $\tau_{w-perpendicular}$ and $\tau_{w-parallel}$, of the nanotube is proportional to $2/\pi$ times the nanotube aspect ratio. That means that there is a factor of about ~ 94 between the two organizations: a parallel orientation covers the droplet surface with considerably less imo-CH_3 per surface unit.

Understanding the behavior of Imo-CH_3 nanotubes at the interfacial layer is therefore necessary to fully describe imogolite-stabilized O/W emulsion.

3.2. Behavior of Imo-CH_3 nanotubes at the oil-water interface

The volume fraction of oil and water and the organization of the nanotubes can be inferred from their X-ray scattering signature. Emulsions were introduced in capillaries and characterized at mesoscale by SAXS and WAXS. The initial phases in equilibrium (Imo-CH_3 suspension and oil) were also measured under the same conditions. On the scattering diagram of the emulsion at high scattering vector (WAXS), the contributions of the water and the hexadecane are identified by the broad peaks centered at 1.98 $Å^{-1}$ and 1.39 $Å^{-1}$, respectively (Fig. 4, red crosses). This part of the diagram is only sensitive to the water and oil contribution of the emulsion, as the scattering signal in this region could be reproduced by a weighted sum of the oil (orange) and imogolite suspension (blue) scattering diagrams (black curve): $a\ I_{imo\ susp} + b\ I_{Hexadecane}$ where I is the intensity and the volume fraction parameters a and b were found to be 0.48 and 0.55, respectively. The coefficients of a and b used for the sum could be related to the volume fraction of each component in the scattering volume. This sum also reproduces the emulsion scattering patterns until q equal to 10^{-2} $Å^{-1}$, including the region typical of imogolite signature. The volume fractions inferred by SAXS/WAXS (Fig. 4) and from the creaming experiments (Fig. 2) are different. This can result from an additional creaming of the emulsion imposed by the manipulation of the sample when injected in a thin capillary for SAXS/WAXS analysis.

However, while the linear combination of suspension and oil scattered perfectly reproduced the WAXS part of the measured sample, it was not able to reproduce the low part of the SAXS region (below 10^{-2} $Å^{-1}$). Here, an excess of scattering was observed for the emulsion with respect to the Imo-CH_3 suspension in water indicating aggregation of Imo-CH_3. This is a clear signature of the affinity between the Imo-CH_3 nanotubes and the oil phase that favors the formation of larger structures (aggregates).

To go deeper in the understanding of the interfacial behavior of imo-CH_3 at oil/water interface, macroscopic interfaces were analyzed using another alkane (dodecance) in place of hexadecane to avoid oil crystallization at ambient temperature.

The impact of the contact between the oil and the aqueous Imo-CH_3 suspension was also observed macroscopically using the pendant drop technique. Droplets of a 0.6 wt% Imo-CH suspension (30 μL) were quickly injected into dodecane, then slowly withdrawn back at a rate of 2.5 $\mu L{\cdot}s^{-1}$ after contact times of 5, 30 and 300 s (Fig. 5). When the droplets were contracted, a buckling effect, such as wrinkles appeared at the interface, evidencing the formation of a solid film even after 5 s of contact. The wrinkles appeared earlier with longer contact time between the aqueous solution and the oil. The layer also seems to get thicker over time, and the video recording of droplet contraction clearly reveals a change from liquid to solid state at the interface (see Video S9). Such effects have already been observed for water droplets in crude oil [54], for asphaltene stabilized emulsions [55,56] and for colloidal particles [57]. It has been interpreted by the formation of a cross-linked gel at the oil–water interface [54–57]. Buckling effects are also typical in attractive Pickering emulsion gels [58] and in deflated elastic capsules adsorbed at an oil/water interface [59].

Hybrid imogolites stabilize the interface around the droplet as soon as a critical concentration is reached (Fig. 3). Fig. 5 demonstrates that this stabilization happens very quickly by adsorption of the imogolites at the water/oil interface leading to the creation of a film that evolves into a solid-like layer between the two environments (aqueous and organic). This film lowers the interfacial tension, where it first decreases over minutes, and then slows down to reach a plateau (see in **Figure S10**). This is a typical behavior observed for a two-step particle adsorption driven first by diffusion and then by non-diffusion-controlled kinetics

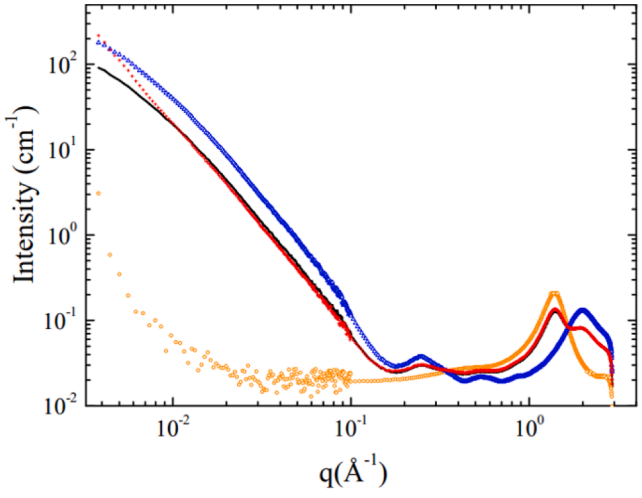

Fig. 4. SAXS/WAXS diagrams of an aqueous hybrid imogolite suspension (blue triangles), hexadecane oil (orange circles) and the emulsion (red crosses), as well as a reconstruction of the SAXS/WAXS diagram of the emulsion by a sum of the scattering of the initial components (black line): a $I_{imo\ susp}$ + b $I_{Hexadecane}$. The emulsion was prepared with 50 $\%_{v/v}$ aqueous suspension of hybrid imogolites at 0.6 wt % of imogolite and 50 $\%_{v/v}$ hexadecane. The parameters are equal to a = 0.48 and b = 0.55. (For interpretation of the references to color in this figure legend, the reader is referred to the web version of this article.)

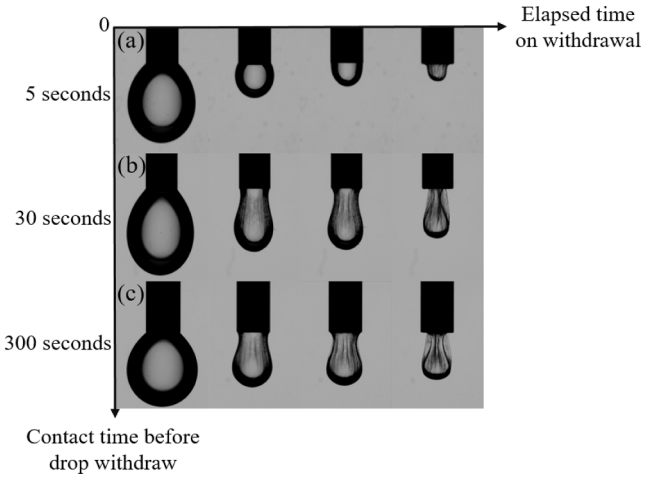

Fig. 5. Drops of a hybrid imogolite suspension injected from a needle immersed in dodecane. Snapshots of contraction after three different contact times (t_0) before withdrawing of the water suspension at 2.5 $\mu L{\cdot}s^{-1}$: (a) t_0 = 5-seconds, (b) t_0 = 30-seconds and (c) t_0 = 300-seconds contact time. The vertical axis corresponds to the contact time between the hybrid imogolite suspension drop and the dodecane environment phase, this step is done before the drop withdrawal. The horizontal axis corresponds to the time elapsed during the drop withdrawal, in ascending order.

with a potential reorganization or a relaxation of the particles at and around the interface (reorientation or formation of a gel or a thick interface) [60]. In the case of proteins described by C.J. Beverung et al, such behavior has been related to the formation of a viscoelastic film [60]. In the case of asphaltene, the behavior at high interfacial coverage has also been explained by a barrier adsorption-controlled regime [61]. We can conclude that hybrid imogolites adsorb quickly at the interface and that reorganization, leading to more aggregated nanotubes as revealed by SAXS, occurs at a later stage.

To better understand the impact of the organization of the imogolites at the interface, the mechanical response of the emulsions was tested immediately after preparation and after aging times of 1 h and 168 h (one week). The elastic and viscous responses of the emulsion during a strain sweep, given by the storage modulus (G′) and loss modulus (G″), respectively, are presented **in** Fig. 6 for different aged emulsions.

As observed **in** Fig. 6**a**, both moduli are constant at low strain, reflecting a linear viscoelastic behavior. The storage modulus is higher than the loss modulus until reaching a critical strain for G′ = G″ where the emulsion starts to flow. In the linear regime, the frequency sweep (see **Figure S5**) shows that the material is significantly more elastic than viscous when small deformations are applied, as evidenced by the storage modulus (G′) being at least an order of magnitude larger than the loss modulus (G″) over the entire range of frequencies studied. We can notice also that the extent of the linear viscoelastic domain is significantly higher for mature emulsions reflecting the reinforcement of the material over time as also observed by the increase of the elastic modulus (G′). For example, for 0.01 % strain, G' is equal to 46 Pa, 192 Pa and 374 Pa for emulsions made respectively at t = 0 h, t = 1 h and t = 1 week. This result is consistent with the gel/solid layer characteristics developing within the emulsion in which hybrid imogolites organize and reorganize through diffusion into the aqueous phase to make a percolating network [62–73]. Even though such an interpretation is described in systems made of clay, such as laponite, halloysite or bentonite [5,30,62,74–77], the mechanism is very different in the case of Imo-CH_3, where the gel phase propagates into the continuous phase due to the confinement of oil inside imogolite nanotubes forming a sticky gel interface. The imogolite network is consolidated over time by entanglements of nanotubes, thus, the solid layer at the interface of the droplets evolves and expands until it reaches a certain stiffness. When emulsions were exposed to low strains, the viscoelastic modulus are large and they cannot flow spontaneously. In this way, a yield stress (τ) may by defined from the crossover point between G′ and G″. Thus, Fig. 6**b** presents the shear stress as a function of the strain and we found yield stress values of τ egal to 0.6 Pa, τ = 5 Pa and τ = 12 Pa for emulsions aged for t = 0 h, t = 1 h and t = 1 week, respectively.

Curve profiles in Fig. 6**b** and the photography in **Figure S11** showing the emulsion after deformation provide information regarding the system. It is typical of a yield stress fluid [78,79]. This property can be directly bound to the thixotropic character of clay minerals, such as montmorillonite, kaolinite, halloysite and hybrid imogolite, which is reflected in the emulsion [80,81]. Furthermore, hybrid imogolite thixotropy increases with increasing imogolite mass concentration due to the nanotubes aggregation [82].

3.3. *Coalescence mechanism*

As discussed in a previous section, the coalescence mechanism is connected to the mass concentration of nanotubes in the emulsion. Indeed, if this concentration is large enough to reach the required critical surface concentration of the oil droplet, then coalescence is blocked, whereas at low concentration, coalescence may occur. The mechanism of coalescence can be explained by energetic arguments.

For spherical nanoparticles, the variation of energy due to the transfer from the water phase to the oil/water interface is given by Eq (3): [6,17].

$$\Delta E = \gamma \pi r_{NP}^2 (1 - \cos(\theta))^2 \quad (3)$$

with γ the interfacial tension between oil and water, r_{NP} the nanoparticle radius and θ the contact angle of the nanoparticle at the oil–water interface. It turns out to be very large even for small nanoparticles. For example, with r_{NP} = 10 nm, $\theta = 90°$ and γ = 49 mJ·m^{-2} [83], we obtain $\Delta E > 1000kT$. Therefore, the adsorption is considered as irreversible. With irreversibly attached nanoparticles, when two droplets, *1* and *2* (with radius r_1 and r_2), are not sufficiently covered to prevent their coalescence, the resulting larger droplet, *3*, has a higher mass coverage per surface unit, τ_3, which can be calculated from the mass coverage per surface unit, τ_i, of initial droplets (Eq. (4).

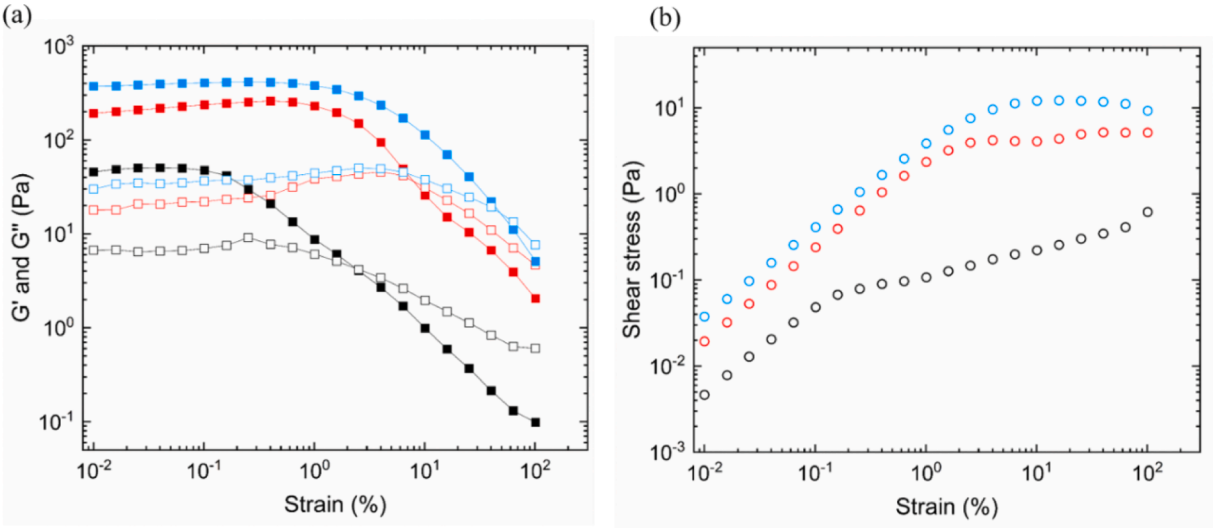

Fig. 6. Strain amplitude sweep measurement of an emulsion of 40 %v/v aqueous Imo-CH3 suspension (2.5 wt%) and 60 %v/v hexadecane mixed for 3 min at 25,000 rpm. These values allow the incorporation of the maximum amount of oil in the emulsion. (a) Full and empty squares indicate, the storage module G' and the loss module G'' respectively. (b) Circles show the strain stress evolution. Three samples have been prepared and stored at 20°c in a close vessel. After a defined aging time the emulsion is sampled for analysis. Comparison of t = 0 (black lines and symbols), t = 1 h (red lines and symbols) and at t = 168 h (blue lines and symbols) aging times. The measurement was performed for a strain of 1 × 10–4 to 1 (0.01 to 100 %) and an angular range of 1 rad·s-1. (For interpretation of the references to color in this figure legend, the reader is referred to the web version of this article.)

$$\tau_3 = \frac{\left(r_1^2 \tau_1 + r_2^2 \tau_2\right)}{\left(r_1^3 + r_2^3\right)^{2/3}} \quad (4)$$

Using equation (4), it appears that for two identical droplets with a coverage, τ_0, τ_3 is simply equal to 1.26 τ_0. In such a system, no excess oil phase is released and the final size of the droplets is controlled by the initial concentration of nanoparticles [10]. For Imo–CH_3 Pickering emulsions, we observed the formation of a solid layer upon adsorption at oil–water interface, but the coalescence mechanism seems to be very different and closer to the one observed by Fouilloux *et al.* for silica nanoparticles [84]. They have proposed that even if the adsorption is strong, the controlling factor to determine if coalescence will be arrested resides in a non-dimensional number (α) which compares the ratio between the energy release per droplet ($\Delta S\,\gamma$) during coalescence to the total surface adhesion energy of the adsorbed particle ($2N\Delta E_a$) with Eq (5):

$$\alpha = \frac{\Delta S\ \gamma}{2\ N\ \Delta E_a} \quad (5)$$

with N, the number of imogolite per droplet calculated from Eq (6)

$$N = \frac{m_{imo}}{m_{imo}^{unit}\ l_{imo}} = \frac{\tau_4 \pi r_{drop}^2}{m_{imo}^{unit} l_{imo}} \quad (6)$$

where m_{imo} is the mass of imogolite around one droplet, m_{imo}^{unit} is the mass of the imogolite per unit length (see Materials and methods: *Synthesis of hybrid imogolites nanotubes and* ***Tables S1 to S3***), τ the mass coverage per surface unit for a droplet of radius r_{drop}. We will use this model as a limit case where all viscoelastic effects are neglected (flow of oil, mechanical properties of the interface…) [11].

If this number (α) is larger than 1, then desorption upon coalescence could be possible [84]. In such a case, right after the coalescence event, the surface coverage of droplets may not increase or could even decrease. Therefore, an initial coalescence may lead to a catastrophic cascade of successive coalescence events entailing the release of an excess of oil phase and Imo-CH_3 nanotubes [85]. During such a catastrophic coalescence cascade, the released nanoparticles can re-adsorb at the oil water interfaces. The release of the excess oil phase, therefore, comes with an increase of the surface coverage of remaining droplets. The process then stops when the critical surface concentration required to prevent coalescence is reached on the remaining droplets, defining a critical surface coverage τ_c. A schematic representation of such a coalescence mechanism is given in Fig. 7. This non-dimensional number (α) is then calculated as a function of the critical coverage rate, τ_c.

In the case of coalescence between two droplets of radius, r_{drop}, the total surface area of the two initial droplets is $S1_{drop} = 8\,\pi\,r_{drop}^2$. Coalesced droplets of radius R will have a larger volume and a lower surface area than the two initial droplets. Thus, the new volume is proportional to R^3, *i.e.,* 2 r_{drop}^3, and the new surface area is equal to $S2_{drop} = 4\,\pi\left(2\,r_{drop}^3\right)^{\frac{2}{3}}$. Using this information, the variation in surface area induced by the coalescence between two droplets ΔS can be calculated as follows (Eq(7)):

$$\Delta S = S2_{drop} - S1_{drop} = 4\,\pi\left(2\,r_{drop}^3\right)^{\frac{2}{3}} - 8\,\pi\,r_{drop}^2 = 4\,\pi\,r_{drop}^2\left(2^{\frac{2}{3}} - 2\right) \quad (7)$$

To estimate the adhesion energy, we consider the case of already oil filled nanotubes as explained in SI (**Figure S12**). In this case, the energy difference between free and droplet-adsorbed nanotubes depends mainly on the exposed oil water interfaces at the tip of the nanotube and on the oil droplet.The adhesion energy would be in this case given by $\Delta E_a = -2\gamma\,\pi\,r_{imo-int}^2$, with $r_{imo-int}$ the internal radius of Imo-CH_3 and γ the oil/water interfacial tension. For a dodecane-water interface and Imo-CH_3, $\gamma = 46$ mJ·m^{-2} and $r_{imo-int} = 0.93$nm, we obtain $\Delta E_a \sim -62kT$ (at 20 °C). For a given mass coverage per surface unit, τ, we thus have:

$$\alpha = \frac{4\,\pi\,r_{drop}^2\left(2^{\frac{2}{3}} - 2\right)\gamma}{2\left(\tau_4 \frac{\pi\,r_{drop}^2}{m_{imo}^{unit} l_{imo}}\right)\left(-2\gamma\,\pi\,r_{imo-int}^2\right)} = \frac{\left(2^{\frac{2}{3}} - 2\right) m_{imo}^{unit} l_{imo}}{-\tau\,4\pi\,r_{imo-int}^2} \quad (8)$$

If α is greater than 1, it means that even though the nanotubes are firmly attached to the interface, the coalescence may release enough energy to detach them and trigger a catastrophic cascade of coalesce events. To determine α, it is thus required to know the τ_c value.

At the end of the coalescence process, the total surface area of the oil droplets is equal to:

$$S = \frac{3\,V_e\,\Phi_j}{R_{drop}} \quad (9)$$

where V_e is the volume of the emulsion and R_{drop} the radius of the droplets. If we assume that all the nanoparticles are adsorbed on the droplet, we have a mass of adsorbed nanoparticle given by $m = \tau_c S$. So the initial concentration, $C_{Imo\text{-}CH3}$, of nanotubes in the total volume is:

$$C_{imo-CH3(g\cdot m^{-3})} = \frac{m}{V_{total}} = \frac{3\tau_c\,\Phi_e\,\Phi_j}{R_{drop}} \quad (10)$$

This concentration has to be transformed into the imogolite concentration in the initial aqueous phase, $C^*_{Imo\text{-}CH3}$:

$$C^*_{imo-CH3} = \frac{3\tau_c\,\Phi_e\,\Phi_j}{R_{drop}(1-\Phi_o)} \quad (11)$$

An estimation of the critical mass coverage per surface unit, τ_c, can be obtained from Fig. 3. This figure suggests a limit between the

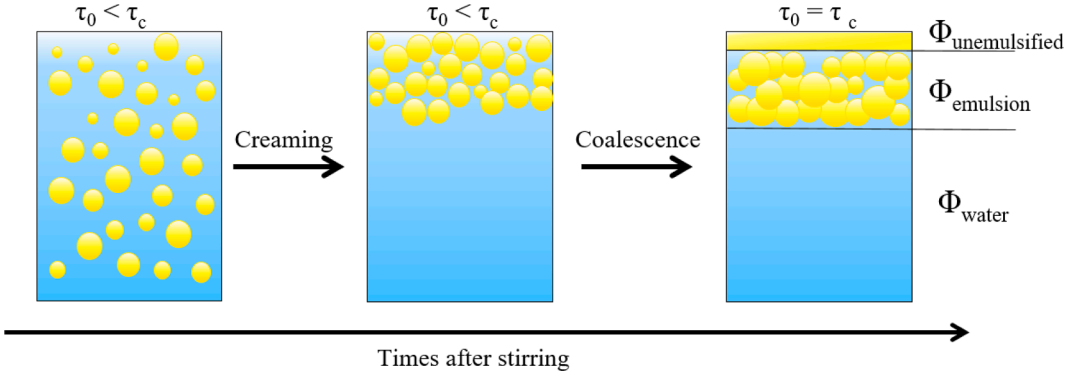

Fig. 7. Schematic representation of the coalescence mechanism: the first step corresponds to the creaming of the drops, and then the second to the coalescence of the drops, causing an increasing size of the oil drops in the vial. At the end of the coalescence, we have a volume fraction of emulsion, $\Phi_{emulsion}$, containing droplets having a critical mass coverage per unit surface, τ_c. The total oil volume fraction is $\Phi_{unemulsified} + \Phi_j\Phi_{emulsion}$ and the total water volume fraction is $\Phi_{water} + (1-\Phi_j)\Phi_{emulsion}$. The non-emulsified flat oil layer is protected by the imogolites because they are also adsorbed at the oil/water interface, which prevents coalescence.

existence of the emulsion in equilibrium with oil in excess and a full emulsification of the oil. When emulsification is fully obtained, the emulsion volume fraction Φ_e is equal to Φ_o/Φ_j. This limit occurs, for example, at $C^*_{Imo\text{-}CH3} \sim 6000$ g·m^{-3}, *i.e.,* 0.6 wt%, and$\Phi_o = 0.5$. It is thus possible to determine$\tau_c \sim 0.025$ g·m^{-2} with $R_{drop} = 12.5 \times 10^{-6}$ m.

This value lies between the perpendicular mass concentration limit of 0.47 g·m^{-2} and the parallel one of 3.9×10^{-3} g·m^{-2}. This means that mixed orientations are probably present on the droplets. With a critical coverage rate, τ_c, of 0.025 g·m^{-2}, the value of α is ~ 5.2 for $l_{imo} = 290$ nm and $r_{imo\text{-}int} = 0.93$ nm. It confirms that the cascade coalescence mechanism is consistent and existing in this particular case.

3.4. Evolution of the solid interfacial layer

To explain the evolution of the emulsion properties over time, we reiterate that imogolites are present in the whole aqueous phase of the emulsion, as presented in Fig. 1. Thus, the oil phase is propagated toward the continuous phase through the nanotube cavity. Therefore, there exists an oil–water interface away from the droplet limit which forms a sticky front of confined oil, also described as a gel. At this front, the Imo-CH_3 nanotubes tend to aggregate, and once attached to the front, the oil can diffuse through the nanotubes contributing to an increase of the gel layer (as a shell) around the oil droplets, as depicted in Fig. 8.

The front most probably grows in the free space between jammed droplets, and thus a continuous network is formed and strengthens over time. This is in line with morphologies observed in Fig. 1 for the confined Nile Red phase, and with the rheological properties in Fig. 6. In comparison to the literature, in our case, the gel is obtained from the contact of the oil with the imogolites without adding any co-surfactants nor stimuli. It is interesting to note that this oil propagation in the dispersed phase is not triggering a fast Oswald ripening of the polydisperse oil droplets. It means that the difference in Laplace pressure from one droplet to the other is not sufficient to move the confined fluid through the nanotubes. If we imagine two droplets of different size $R_1 > R_2$ connected by a single Imo-CH_3 nanotube filled with oil, the pressure difference between the extremities of the nanotube is given by $\Delta P = 2\sigma\left(\frac{1}{R_2} - \frac{1}{R_1}\right)$. Considering the hydrodynamic laws are valid down to the nanometer range, then the flow through the tube would be $Q = \Delta P/R_h$ with R_h the hydraulic resistance of a cylinder ($R_h = \frac{8\,\eta\,l_{imo}}{\pi\, r^4_{imo-int}}$). Taking the dynamic viscosity of hexadecane, η, equal to 3.004×10^{-3} Pa·s at 20 °C, it would take more than 1000 years to empty a 20 μm droplet inside a 50 μm one trough a single nanotube. Obviously, there could be more nanotubes linking two droplets. The analysis of such a confined flow evolution of the emulsion would be extremely interesting and goes far beyond the scope of this paper [86].

In the Pickering emulsion field, clays have been used to prepare oil-in-water emulsions as a green alternative to surfactant-prepared emulsions. Advantage of Pickering emulsion is the formation of a layer able to provide a mechanical barrier against coalescence [87]. When tubular clays are used, an additional phenomenon favors stabilization, for example, Owoseni *et al.* [88] have shown that halloysite particles adsorb at the oil–water interface by their long side, forming a network on the interface through end-to-end linkage. This particular organization stabilizes the emulsion. It is also known that clays can easily form hydrogels [28,89], which can be used to stabilize oil-in-water emulsions through the creation of an organization of the clays in a framework in the aqueous continuous phase [5,16]. In the case of Imo-CH_3, hydrogel formation is triggered by contact between the imogolites and oil. The uniqueness of the stabilization mechanism comes from the propagation of a sticky confined oil front toward the continuous phase, which strengthens the emulsion with time. This example illustrates the complexity resulting from the use of Janus tubular clays for oil-in-water emulsification.

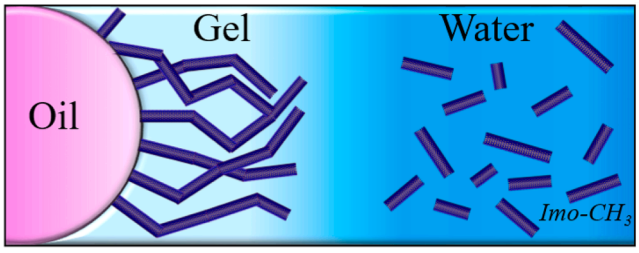

Fig. 8. Drawing illustrating the hypothesis of a sticky confined oil front around a single oil droplet stabilized by an Imo-CH_3 gel. The oil drop is represented in pink and the imogolite gel spreading the oil is represented in dark blue. (For interpretation of the references to color in this figure legend, the reader is referred to the web version of this article.)

4. Conclusions and perspectives

In the field of Pickering emulsion [7,8], original Janus inside/ouside clays nanotubes (hybrid imogolite) [32,33] can be used to form emulsions [44]. However, the stabilization mechanism was not understood. In this paper, we evidence the oil in water nature of the emulsion and explain the particular stabilization mechanism. Imo-CH_3 Janus nanotubes are able to stabilize oil–water emulsions directly after synthesis at very low concentration (critical surface concentration 0.025 g·m^{-2}) and without requiring any addition of salt or surfactants and/or modifying the pH. Interestingly, while Imo-CH_3 form a solid-like layer at the oil–water interface within a few seconds, no typical shape of "arrested" coalescence is observed contrary to classical observation in Pickering emulsion [10,11]. This is interpreted by an unfavorable energy balance between the adhesion of the nanotubes and the energy released during coalescence events. The oil droplets are thus destabilized through catastrophic cascade coalescence events. In comparison to emulsions stabilized by clays [5,16,28,87–89], we demonstrate here that with Imo-CH_3, the oil has a unique behavior in the emulsification process: it is the driver of the observed time evolution of the interfacial solid layer. We interpret this evolution by the propagation of an encapsulated oil front in the disperse phase, which triggers the aggregation of the initially dispersed nanotubes. Imogolite is an emulsifier with two functions: firstly, it helps to stabilize and isolate the droplets, and thereafter, it helps the transport of the oil. The emulsification of oil by Imo-CH_3 opens new possibilities, in particular in photocatalysis, as Imo-CH_3 has been shown to be an effective photocatalytic nanoreactor that can be used to degrade and transform pollutants on a large scale [90]. Emulsification of other halogen or phosphorus organic substances might also be possible, as Imo-CH_3 is efficient for encapsulating a large variety of hydrophobic molecules.

Data availability

Data will be made available on request.

CRediT authorship contribution statement

Estelle Puel: Data curation, Writing - original draft. **Céline Cau Dit Coumes:** Conceptualization, Writing - review & editing. **Arnaud Poulesquen:** Investigation, writing - review editing. **Fabienne Testard:** Supervision, Investigation, Writing - review & editing. **Antoine Thill:** Conceptualization, Supervision, Writing - review & editing.

Declaration of Competing Interest

The authors declare that they have no known competing financial interests or personal relationships that could have appeared to influence the work reported in this paper.

Data availability

Data will be made available on request.

Acknowledgements

The authors gratefully acknowledge the French Alternative Energies and Atomic Energy Commission (CEA) and the FOCUS research program for funding. The authors gracefully thank Dr Mark Levenstein for thorough reading and useful comments.

Appendix A. Supplementary material

Supplementary data to this article can be found online at https://doi.org/10.1016/j.jcis.2023.04.102.

References

[1] D. Georgieva, V. Schmitt, F. Leal-Calderon, D. Langevin, On the Possible Role of Surface Elasticity in Emulsion Stability, Langmuir 25 (2009) 5565–5573, https://doi.org/10.1021/la804240e.
[2] C. Mabille, F. Leal-Calderon, J. Bibette, V. Schmitt, Monodisperse fragmentation in emulsions: Mechanisms and kinetics, Europhys. Lett. 61 (2003) 708–714, https://doi.org/10.1209/epl/i2003-00133-6.
[3] L. Zhang, Q. Lei, J. Luo, M. Zeng, L. Wang, D. Huang, X. Wang, S. Mannan, B. Peng, Z. Cheng, Natural Halloysites-Based Janus Platelet Surfactants for the Formation of Pickering Emulsion and Enhanced Oil Recovery, Sci. Rep. 9 (2019) 163, https://doi.org/10.1038/s41598-018-36352-w.
[4] C. Mabille, V. Schmitt, P. Gorria, F.L. Calderon, V. Faye, B. Deminiere, J. Bibette, Rheological and Shearing Conditions for the Preparation of Monodisperse Emulsions, Langmuir 16 (2000) 422–429, https://doi.org/10.1021/la990850w.
[5] D. Kpogbemabou, G. Lecomte-Nana, A. Aimable, M. Bienia, V. Niknam, C. Carrion, Oil-in-water Pickering emulsions stabilized by phyllosilicates at high solid content, Colloids Surf. A Physicochem. Eng. Asp. 463 (2014) 85–92, https://doi.org/10.1016/j.colsurfa.2014.09.037.
[6] Y. Chevalier, M.-A. Bolzinger, Emulsions stabilized with solid nanoparticles: Pickering emulsions, Colloids Surf. A Physicochem. Eng. Asp. 439 (2013) 23–34, https://doi.org/10.1016/j.colsurfa.2013.02.054.
[7] B.P. Binks, S.O. Lumsdon, Pickering Emulsions Stabilized by Monodisperse Latex Particles: Effects of Particle Size, Langmuir 17 (2001) 4540–4547, https://doi.org/10.1021/la0103822.
[8] B.P. Binks, J.H. Clint, Solid Wettability from Surface Energy Components: Relevance to Pickering Emulsions, Langmuir 18 (2002) 1270–1273, https://doi.org/10.1021/la011420k.
[9] E. Vignati, R. Piazza, T.P. Lockhart, Pickering Emulsions: Interfacial Tension, Colloidal Layer Morphology, and Trapped-Particle Motion, Langmuir 19 (2003) 6650–6656, https://doi.org/10.1021/la034264l.
[10] S. Arditty, C.P. Whitby, B.P. Binks, V. Schmitt, F. Leal-Calderon, Some general features of limited coalescence in solid-stabilized emulsions, Eur. Phys. J. E 11 (2003) 273–281, https://doi.org/10.1140/epje/i2003-10018-6.
[11] A.B. Pawar, M. Caggioni, R. Ergun, R.W. Hartel, P.T. Spicer, Arrested coalescence in Pickering emulsions, Soft Matter 7 (2011) 7710, https://doi.org/10.1039/c1sm05457k.
[12] B.P. Binks, W. Cho, P.D.I. Fletcher, D.N. Petsev, Stability of Oil-in-Water Emulsions in a Low Interfacial Tension System, Langmuir 16 (2000) 1025–1034, https://doi.org/10.1021/la990952m.
[13] B.P. Binks, J.A. Rodrigues, Double Inversion of Emulsions By Using Nanoparticles and a Di-Chain Surfactant, Angew. Chem. Int. Ed. 46 (2007) 5389–5392, https://doi.org/10.1002/anie.200700880.
[14] A.D. Dinsmore, M.F. Hsu, M.G. Nikolaides, M. Marquez, A.R. Bausch, D.A. Weitz, Colloidosomes: Selectively Permeable Capsules Composed of Colloidal Particles, Science 298 (2002) 1006–1009, https://doi.org/10.1126/science.1074868.
[15] M. in het Panhuis, V.N. Paunov, Assembling carbon nanotubosomes using an emulsion-inversion technique, Chem. Commun. (13) (2005) 1726.
[16] X. Cai, C. Li, Q. Tang, B. Zhen, X. Xie, W. Zhu, C. Zhou, L. Wang, Assembling kaolinite nanotube at water/oil interface for enhancing Pickering emulsion stability, Appl. Clay Sci. 172 (2019) 115–122, https://doi.org/10.1016/j.clay.2019.02.021.
[17] R. Aveyard, B.P. Binks, J.H. Clint, Emulsions stabilised solely by colloidal particles, Adv. Colloid Interface Sci. 100–102 (2003) 503–546, https://doi.org/10.1016/S0001-8686(02)00069-6.
[18] M. Destribats, V. Lapeyre, M. Wolfs, E. Sellier, F. Leal-Calderon, V. Ravaine, V. Schmitt, Soft microgels as Pickering emulsion stabilisers: role of particle deformability, Soft Matter 7 (2011) 7689, https://doi.org/10.1039/c1sm05240c.
[19] X. Feng, H. Dai, L. Ma, Y. Fu, Y. Yu, H. Zhou, T. Guo, H. Zhu, H. Wang, Y. Zhang, Properties of Pickering emulsion stabilized by food-grade gelatin nanoparticles: influence of the nanoparticles concentration, Colloids Surf. B Biointerfaces 196 (2020), 111294, https://doi.org/10.1016/j.colsurfb.2020.111294.
[20] N. Ghavidel, P. Fatehi, Pickering/Non-Pickering Emulsions of Nanostructured Sulfonated Lignin Derivatives, ChemSusChem 13 (2020) 4567–4578, https://doi.org/10.1002/cssc.202000965.
[21] D. Gonzalez Ortiz, C. Pochat-Bohatier, J. Cambedouzou, M. Bechelany, P. Miele, Current Trends in Pickering Emulsions: Particle Morphology and Applications, Engineering 6 (2020) 468–482, https://doi.org/10.1016/j.eng.2019.08.017.
[22] J. Zhou, X. Qiao, B.P. Binks, K. Sun, M. Bai, Y. Li, Y. Liu, Magnetic Pickering Emulsions Stabilized by Fe3O4 Nanoparticles, Langmuir 27 (2011) 3308–3316, https://doi.org/10.1021/la1036844.
[23] D. Langevin, J.-F. Argillier, Interfacial behavior of asphaltenes, Adv. Colloid Interface Sci. 233 (2016) 83–93, https://doi.org/10.1016/j.cis.2015.10.005.
[24] S. Parajuli, A.L. Dorris, C. Middleton, A. Rodriguez, M.O. Haver, N.I. Hammer, E. Ureña-Benavides, Surface and Interfacial Interactions in Dodecane/Brine Pickering Emulsions Stabilized by the Combination of Cellulose Nanocrystals and Emulsifiers, Langmuir 35 (2019) 12061–12070, https://doi.org/10.1021/acs.langmuir.9b01218.
[25] H. Dupont, V. Maingret, V. Schmitt, V. Héroguez, New Insights into the Formulation and Polymerization of Pickering Emulsions Stabilized by Natural Organic Particles, Macromolecules 54 (2021) 4945–4970, https://doi.org/10.1021/acs.macromol.1c00225.
[26] A. Perro, F. Meunier, V. Schmitt, S. Ravaine, Production of large quantities of “Janus” nanoparticles using wax-in-water emulsions, Colloids Surf A Physicochem Eng Asp 332 (2009) 57–62, https://doi.org/10.1016/j.colsurfa.2008.08.027.
[27] G. Lazzara, G. Cavallaro, A. Panchal, R. Fakhrullin, A. Stavitskaya, V. Vinokurov, Y. Lvov, An assembly of organic-inorganic composites using halloysite clay nanotubes, Curr. Opin. Colloid Interface Sci. 35 (2018) 42–50, https://doi.org/10.1016/j.cocis.2018.01.002.
[28] L. Lisuzzo, G. Cavallaro, F. Parisi, S. Milioto, G. Lazzara, Colloidal stability of halloysite clay nanotubes, Ceram. Int. 45 (2019) 2858–2865, https://doi.org/10.1016/j.ceramint.2018.07.289.
[29] N.P. Ashby, B.P. Binks, Pickering emulsions stabilised by Laponite clay particles, PCCP 2 (2000) 5640–5646, https://doi.org/10.1039/b007098j.
[30] S. Abend, N. Bonnke, U. Gutschner, G. Lagaly, Stabilization of emulsions by heterocoagulation of clay minerals and layered double hydroxides, Colloid Polym. Sci. 276 (1998) 730–737, https://doi.org/10.1007/s003960050303.
[31] G. Lagaly, M. Reese, S. Abend, Smectites as colloidal stabilizers of emulsions, Appl. Clay Sci. 14 (1-3) (1999) 83–103.
[32] L. Lisuzzo, G. Cavallaro, F. Parisi, S. Riela, S. Milioto, G. Lazzara, Colloidal stability and self-assembling behavior of nanoclays, in: Clay Nanoparticles, Elsevier, 2020: pp. 95–116. https://doi.org/10.1016/B978-0-12-816783-0.00004-9.
[33] G. Cavallaro, G. Lazzara, S. Milioto, F. Parisi, Hydrophobically Modified Halloysite Nanotubes as Reverse Micelles for Water-in-Oil Emulsion, Langmuir 31 (2015) 7472–7478, https://doi.org/10.1021/acs.langmuir.5b01181.
[34] N. Yoshinaga, S. Aomine, Imogolite in some ando soils, Soil Science and Plant, Nutrition 8 (1962) 22–29, https://doi.org/10.1080/00380768.1962.10430993.
[35] P.D.G. Cradwick, V.C. Farmer, J.D. Russell, C.R. Masson, K. Wada, N. Yoshinaga, Imogolite, a Hydrated Aluminium Silicate of Tubular Structure, Nature Physical, Science 240 (1972) 187–189, https://doi.org/10.1038/physci240187a0.
[36] V.C. Farmer, A.R. Fraser, J.M. Tait, Synthesis of imogolite: a tubular aluminium silicate polymer, J. Chem. Soc. Chem. Commun. (1977) 462, https://doi.org/10.1039/c39770000462.
[37] V.C. Farmer, M.J. Adams, A.R. Fraser, F. Palmieri, Synthetic imogolite: properties, synthesis and possible applications, Clay Miner. 18 (1983) 459–472, https://doi.org/10.1180/claymin.1983.018.4.11.
[38] L.A. Bursill, J.L. Peng, L.N. Bourgeois, Imogolite: An aluminosilicate nanotube material, Philos. Mag. A 80 (2000) 105–117, https://doi.org/10.1080/01418610008212043.
[39] I. Bottero, B. Bonelli, S.E. Ashbrook, P.A. Wright, W. Zhou, M. Tagliabue, M. Armandi, E. Garrone, Synthesis and characterization of hybrid organic/inorganic nanotubes of the imogolite type and their behaviour towards methane adsorption, PCCP 13 (2011) 744–750, https://doi.org/10.1039/C0CP00438C.
[40] M.S. Amara, E. Paineau, S. Rouzière, B. Guiose, M.-E.-M. Krapf, O. Taché, P. Launois, A. Thill, Hybrid, Tunable-Diameter, Metal Oxide Nanotubes for Trapping of Organic Molecules, Chem. Mater. 27 (2015) 1488–1494, https://doi.org/10.1021/cm503428q.
[41] P. Picot, F. Gobeaux, T. Coradin, A. Thill, Dual internal functionalization of imogolite nanotubes as evidenced by optical properties of Nile red, Appl. Clay Sci. 178 (2019), 105133, https://doi.org/10.1016/j.clay.2019.105133.
[42] M.-C. Pignié, S. Patra, L. Huart, A.R. Milosavljević, J.P. Renault, J. Leroy, C. Nicolas, O. Sublemontier, S. Le Caër, A. Thill, Experimental determination of the curvature-induced intra-wall polarization of inorganic nanotubes, Nanoscale 13 (2021) 19650–19662, https://doi.org/10.1039/D1NR06462B.
[43] R. Nasi, F. Sannino, P. Picot, A. Thill, O. Oliviero, S. Esposito, M. Armandi, B. Bonelli, Hybrid organic-inorganic nanotubes effectively adsorb some organic pollutants in aqueous phase, Appl. Clay Sci. 186 (2020) 105449.
[44] P. Picot, O. Taché, F. Malloggi, T. Coradin, A. Thill, Behaviour of hybrid inside/out Janus nanotubes at an oil/water interface. A route to self-assembled nanofluidics? Faraday Discuss. 191 (2016) 391–406, https://doi.org/10.1039/C6FD00034G.
[45] P. Picot, Y. Liao, E. Barruet, F. Gobeaux, T. Coradin, A. Thill, Exploring Hybrid Imogolite Nanotube Formation via Si/Al Stoichiometry Control, Langmuir 34 (2018) 13225–13234, https://doi.org/10.1021/acs.langmuir.8b01075.
[46] CEA-IRAMIS-LIONS, Python for Small Angle X-ray Scattering data acquisition, treatment and computation of model SAXS intensities., (n.d.). https://pypi.org/project /pySAXS/.
[47] O. Taché, S. Rouzière, P. Joly, M. Amara, B. Fleury, A. Thill, P. Launois, O. Spalla, B. Abécassis, MOMAC: a SAXS/WAXS laboratory instrument dedicated to nanomaterials, J. Appl. Cryst. 49 (2016) 1624–1631, https://doi.org/10.1107/S1600576716012127.

[48] A.B. Hopkins, F.H. Stillinger, S. Torquato, Dense sphere packings from optimized correlation functions, Phys. Rev. E 79 (2009), 031123, https://doi.org/10.1103/PhysRevE.79.031123.
[49] F. Leal-Calderon, F. Thivilliers, V. Schmitt, Structured emulsions, Curr. Opin. Colloid Interface Sci. 12 (2007) 206–212, https://doi.org/10.1016/j.cocis.2007.07.003.
[50] S. Torquato, T.M. Truskett, P.G. Debenedetti, Is Random Close Packing of Spheres Well Defined? Phys. Rev. Lett. 84 (2000) 2064–2067, https://doi.org/10.1103/PhysRevLett.84.2064.
[51] K. Gotoh, J.L. Finney, Statistical geometrical approach to random packing density of equal spheres, Nature 252 (1974) 202–205, https://doi.org/10.1038/252202a0.
[52] M. Clusel, E.I. Corwin, A.O.N. Siemens, J. Brujić, A 'granocentric' model for random packing of jammed emulsions, Nature 460 (2009) 611–615, https://doi.org/10.1038/nature08158.
[53] C.V. Nikiforidis, E. Scholten, High internal phase emulsion gels (HIPE-gels) created through assembly of natural oil bodies, Food Hydrocoll. 43 (2015) 283–289, https://doi.org/10.1016/j.foodhyd.2014.05.030.
[54] A. Yeung, T. Dabros, J. Czarnecki, J. Masliyah, On the interfacial properties of micrometre–sized water droplets in crude oil, Proc. R. Soc. Lond. A 455 (1990) (1999) 3709–3723.
[55] H.W. Yarranton, H. Hussein, J.H. Masliyah, Water-in-Hydrocarbon Emulsions Stabilized by Asphaltenes at Low Concentrations, J. Colloid Interface Sci. 228 (2000) 52–63, https://doi.org/10.1006/jcis.2000.6938.
[56] A. Yeung, L. Zhang, Shear Effects in Interfacial Rheology and Their Implications on Oscillating Pendant Drop Experiments, Langmuir 22 (2006) 693–701, https://doi.org/10.1021/la051795w.
[57] F. Gautier, M. Destribats, R. Perrier-Cornet, J.-F. Dechézelles, J. Giermanska, V. Héroguez, S. Ravaine, F. Leal-Calderon, V. Schmitt, Pickering emulsions with stimulable particles: from highly- to weakly-covered interfaces, PCCP 9 (2007) 6455, https://doi.org/10.1039/b710226g.
[58] B. Wu, C. Yang, Q. Xin, L. Kong, M. Eggersdorfer, J. Ruan, P. Zhao, J. Shan, K. Liu, D. Chen, D.A. Weitz, X. Gao, Attractive Pickering Emulsion Gels, Adv. Mater. 33 (2021) 2102362, https://doi.org/10.1002/adma.202102362.
[59] S. Knoche, D. Vella, E. Aumaitre, P. Degen, H. Rehage, P. Cicuta, J. Kierfeld, Elastometry of Deflated Capsules: Elastic Moduli from Shape and Wrinkle Analysis, Langmuir 29 (2013) 12463–12471, https://doi.org/10.1021/la402322g.
[60] C.J. Beverung, C.J. Radke, H.W. Blanch, Protein adsorption at the oil/water interface: characterization of adsorption kinetics by dynamic interfacial tension measurements, Biophysical Chemistry 81 (1999) 59–80.
[61] J.P. Rane, D. Harbottle, V. Pauchard, A. Couzis, S. Banerjee, Adsorption Kinetics of Asphaltenes at the Oil-Water Interface and Nanoaggregation in the Bulk, Langmuir 28 (2012) 9986–9995, https://doi.org/10.1021/la301423c.
[62] J.L. Dávila, M.A. d'Ávila, Laponite as a rheology modifier of alginate solutions: Physical gelation and aging evolution, Carbohydr. Polym. 157 (2017) 1–8, https://doi.org/10.1016/j.carbpol.2016.09.057.
[63] H.A. Barnes, Rheology of emulsions — a review, Colloids Surf A Physicochem Eng Asp 91 (1994) 89–95, https://doi.org/10.1016/0927-7757(93)02719-U.
[64] S.R. Derkach, Rheology of emulsions, Adv. Colloid Interface Sci. 151 (2009) 1–23, https://doi.org/10.1016/j.cis.2009.07.001.
[65] E. Dickinson, Milk protein interfacial layers and the relationship to emulsion stability and rheology, Colloids Surf. B Biointerfaces 20 (2001) 197–210, https://doi.org/10.1016/S0927-7765(00)00204-6.
[66] T.M. Dreher, J. Glass, A.J. O'Connor, G.W. Stevens, Effect of rheology on coalescence rates and emulsion stability, AIChE J 45 (1999) 1182–1190, https://doi.org/10.1002/aic.690450604.
[67] C. Griffith, H. Daigle, Manipulation of Pickering emulsion rheology using hydrophilically modified silica nanoparticles in brine, J. Colloid Interface Sci. 509 (2018) 132–139, https://doi.org/10.1016/j.jcis.2017.08.100.
[68] D. Langevin, Influence of interfacial rheology on foam and emulsion properties, Adv. Colloid Interface Sci. 88 (2000) 209–222, https://doi.org/10.1016/S0001-8686(00)00045-2.
[69] Y. Lu, X. Qian, W. Xie, W. Zhang, J. Huang, D. Wu, Rheology of the sesame oil-in-water emulsions stabilized by cellulose nanofibers, Food Hydrocoll. 94 (2019) 114–127, https://doi.org/10.1016/j.foodhyd.2019.03.001.
[70] R. Pal, Effect of droplet size on the rheology of emulsions, AIChE J 42 (1996) 3181–3190, https://doi.org/10.1002/aic.690421119.
[71] H.M. Princen, Rheology of Foams and Highly Concentrated Emulsions, J. Colloid Interface Sci. 91 (1983) 16.
[72] L.G. Torres, R. Iturbe, M.J. Snowden, B.Z. Chowdhry, S.A. Leharne, Preparation of o/w emulsions stabilized by solid particles and their characterization by oscillatory rheology, Colloids Surf. A Physicochem. Eng. Asp. 302 (2007) 439–448, https://doi.org/10.1016/j.colsurfa.2007.03.009.
[73] H. Dupont, E. Laurichesse, V. Héroguez, V. Schmitt, Green Hydrophilic Capsules from Cellulose Nanocrystal-Stabilized Pickering Emulsion Polymerization: Morphology Control and Spongelike Behavior, Biomacromolecules 22 (2021) 3497–3509, https://doi.org/10.1021/acs.biomac.1c00581.
[74] K. Suman, M. Mittal, Y.M. Joshi, Effect of sodium pyrophosphate and understanding microstructure of aqueous LAPONITE ® dispersion using dissolution study, J. Phys. Condens. Matter 32 (22) (2020) 224002, https://doi.org/10.1088/1361-648X/ab724d.
[75] R.K. Pujala, N. Joshi, H.B. Bohidar, Spontaneous evolution of self-assembled phases from anisotropic colloidal dispersions, Colloid Polym. Sci. 293 (2015) 2883–2890, https://doi.org/10.1007/s00396-015-3651-3.
[76] Y.M. Joshi, G.R.K. Reddy, A.L. Kulkarni, N. Kumar, R.P. Chhabra, Rheological behaviour of aqueous suspensions of laponite: new insights into the ageing phenomena, Proc. R. Soc. A. 464 (2008) 469–489, https://doi.org/10.1098/rspa.2007.0250.
[77] X. Yue, S.N. Subraveti, G. John, S.R. Raghavan, Phase-Selective Gelation of the Water Phase in an Oil-Water Mixture: An Approach Based on Oil-Activated Nanoparticle Assembly in Water, Langmuir 37 (2021) 8107–8114, https://doi.org/10.1021/acs.langmuir.1c00647.
[78] G. Ovarlez, S. Cohen-Addad, K. Krishan, J. Goyon, P. Coussot, On the existence of a simple yield stress fluid behavior, J. Nonnewton. Fluid Mech. 193 (2013) 68–79, https://doi.org/10.1016/j.jnnfm.2012.06.009.
[79] G. Ovarlez, F. Mahaut, S. Deboeuf, N. Lenoir, S. Hormozi, X. Chateau, Flows of suspensions of particles in yield stress fluids, J. Rheol. 59 (2015) 1449–1486, https://doi.org/10.1122/1.4934363.
[80] N. Khatoon, M.Q. Chu, C.H. Zhou, Nanoclay-based drug delivery systems and their therapeutic potentials, J. Mater. Chem. B 8 (2020) 7335–7351, https://doi.org/10.1039/D0TB01031F.
[81] K. Shikinaka, K. Kaneda, S. Mori, T. Maki, H. Masunaga, Y. Osada, K. Shigehara, Direct Evidence for Structural Transition Promoting Shear Thinning in Cylindrical Colloid Assemblies, Small 10 (2014) 1813–1820, https://doi.org/10.1002/smll.201303360.
[82] W. Baumgarten, J. Dörner, R. Horn, Microstructural development in volcanic ash soils from South Chile, Soil Tillage Res. 129 (2013) 48–60, https://doi.org/10.1016/j.still.2013.01.007.
[83] P.-M. Gassin, G. Martin-Gassin, D. Meyer, J.-F. Dufrêche, O. Diat, Kinetics of Triton-X100 Transfer Across the Water/Dodecane Interface: Analysis of the Interfacial Tension Variation, J. Phys. Chem. C 116 (2012) 13152–13160, https://doi.org/10.1021/jp302514k.
[84] S. Fouilloux, F. Malloggi, J. Daillant, A. Thill, Aging mechanism in model Pickering emulsion, Soft Matter 12 (2016) 900–904, https://doi.org/10.1039/C5SM02134K.
[85] T. Wu, H. Wang, B. Jing, F. Liu, P.C. Burns, C. Na, Multi-body coalescence in Pickering emulsions, Nat. Commun. 6 (2015) 5929, https://doi.org/10.1038/ncomms6929.
[86] L. Bocquet, E. Charlaix, Nanofluidics, from bulk to interfaces, Chem. Soc. Rev. 39 (2010) 1073–1095, https://doi.org/10.1039/B909366B.
[87] F. Leal-Calderon, V. Schmitt, Solid-stabilized emulsions, Curr. Opin. Colloid Interface Sci. 13 (2008) 217–227, https://doi.org/10.1016/j.cocis.2007.09.005.
[88] O. Owoseni, E. Nyankson, Y. Zhang, S.J. Adams, J. He, G.L. McPherson, A. Bose, R. B. Gupta, V.T. John, Release of Surfactant Cargo from Interfacially-Active Halloysite Clay Nanotubes for Oil Spill Remediation, Langmuir 30 (2014) 13533–13541, https://doi.org/10.1021/la503687b.
[89] L.Z. Zhao, C.H. Zhou, J. Wang, D.S. Tong, W.H. Yu, H. Wang, Recent advances in clay mineral-containing nanocomposite hydrogels, Soft Matter 11 (48) (2015) 9229–9246.
[90] S. Patra, D. Schaming, P. Picot, M.-C. Pignié, J.-B. Brubach, L. Sicard, S. Le Caër, A. Thill, Inorganic nanotubes with permanent wall polarization as dual photo-reactors for wastewater treatment with simultaneous fuel production, Environ. Sci. Nano 8 (2021) 2523–2541, https://doi.org/10.1039/D1EN00405K.